Electrodeposited Platinum Nanoparticles on Highly Ordered Titanium Dioxide Nanotubes for Photocatalytic Application: Enhancement of Photocatalytic Degradation of Amido Black Dye

M. A. Hajjaji, K. Missaoui, K. Trabelsi, Abdelkrim Bouzaza, B. Bessais, A. Hajjaji, Aymen Amine Assadi

Platinum nanoparticles decorated TiO_2 nanotubes for VOCs and bacteria removal in simulated real condition: Effect of the deposition method on the photocatalytic degradation process efficiency.

M.A.Hajjaji[a,b,c], K.Missaoui[a], K.Trabelsi[a], A.Bouzaza[b], A.Hajjaji[a], B.Bessais[a], A.A.Assadi[d]

[a]Laboratoire de Photovoltaïque, Centre de Recherches et des Technologies de l'Energie, Technopole de Borj-Cédria, BP 95, 2050 Hammam-Lif, Tunisia

[b]Ecole Nationale Supérieure de Chimie de Rennes, University of Rennes, CNRS, ISCR—UMR6226, 35000 Rennes, France

[c]Faculté des sciences de Tunis, Université de Tunis El Manar, BP 94, Rommana, 1068 Tunis, Tunisia

[d]College of Engineering, Imam Mohammad Ibn Saud Islamic University, IMSIU, Riyadh 11432, Saudi Arabia

* Corresponding authors E-mail address: AAAssadi@imamu.edu.sa; Aymen.assadi@ensc-rennes.fr (Aymen Amin ASSADI).

Abstract

The incorporation of noble metals onto TiO_2 nanostructure is considered as a promoting method to enhance the photocatalytic degradation of pollutant in air treatment process. In this study, highly organized TiO_2 nanotubes (NTs) were grown by the anodization method of Titanium substrates. The TiO_2-NTs were successfully decorated by platinum (Pt) nanoparticles (NPs) using two different deposition methods: (1) electrodeposition and (2) photodeposition.

We explore the impact of different deposition methods on the morphology of Pt nanoparticles (NPs) dispersed onto TiO_2 nanotubes and the optical characteristics of Pt-TiO_2 nanocomposites, investigating their efficacy in photocatalytic degradation We investigate the effect of varying the deposition method on the morphology of Pt-NPs dispersed onto TiO_2 nanotubes and the optical properties of the Pt-TiO_2 nanocomposites and their efficient photocatalytic activity degradation against Volatile Organic Compounds (VOCs) and bacteria. Scanning and Transmission Electron Microscopy (SEM and TEM) reveal a nanotubular TiO_2 anatase structure adorned

with Pt NPs, with the quantity and size of NPs contingent upon the deposition technique employed. The photoluminescence (PL) spectra demonstrate that the Pt/TiO_2 heterojunction facilitates the separation of photogenerated charges, thereby diminishing carrier recombination rates. To point out the effect of Pt NPS, both pure TiO_2 and Pt/TiO_2 heterojunction were tested in the photodegradation of Ethyl Acetate (EA). The Pt/TiO_2 heterojunction exhibits superior photocatalytic performance compared to TiO_2 in EA degradation, regardless of the Pt deposition method employed. Optimal results are achieved with 120 seconds of Pt electrodeposition and 3 hours of Pt photodeposition under visible irradiation, yielding kinetic constants of approximately 0.245 and 0.195 $mg.m^{-3}.s^{-1}$, respectively, underscoring the pivotal role of the platinum deposition method in pollutant photodegradation. Respectively simultaneous removal of EA and bacteria (Escherichia coli) was tested using Pt and non-Pt decorated TiO_2 NTs. We attributed a total degradation of the bacteria after 180 minutes using the two efficient photocatalysts Electro 120 s and Photo 3 hours compared to 60% of degradation using pure TiO_2 nanotubes.

Keywords: TiO_2 nanotubes, Platinum, Photodeposition, Electrodeposition, Indoor air treatment, Photocatalysis, VOCs, Bacteria.

I. Introduction

Humans spend more than 80% of their time in enclosed spaces and breathe on average 14 m^3 of air per day [1]. However, many pollutants are present in the air such as volatile organic compounds (VOCs), inorganic gases (NOx, SOx, O_3), allergenic compounds and microorganisms (bacteria, viruses) and natural biological barriers of the human organism allow them to pass through [2,3]. This air pollution can harm the ecosystem and human health. Indoor air is generally more conducive to these pollutants than outdoor air because outdoor air is dispersed and washed daily by rain and wind, unlike indoor air [4]. Not all VOCs can be removed by the natural environment or by conventional air treatment processes such as solid adsorption [5]. In recent years, indoor air pollution has become a problem raised by numerous

scientific studies [6–8]. In this context, different techniques have been developed to allow the purification of a closed place and advanced oxidation processes (AOP) (photocatalysis, ozonation, nonthermal plasma) have aroused a lot of interest due to their strong capacity to oxidize pollutants [9–11].

Among all these various techniques, photocatalysis is the most promising oxidation technique. This method is based on the decomposition of pollutants by reactive species following photoexcitation of the photocatalyst [12]. The photoelectrochemical behavior of wide gap metal oxide semiconductors was studied by Fujishima [13]. Subsequently, research expanded to test several semiconductors such as ZnO [14], TiO_2 [15], SnO_2 [16], Cu_2O [17] and ZrO_2 [18] irradiated with UV and visible light to obtain the highest performance [19]. Indeed, the photocatalytic processes that involve TiO_2 to be irradiated by UV light showed to be potentially useful and advantageous for air treatment [20]. Due to its high chemical stability, large earth reserves and strong photoactivity, mainly under UV irradiation, it is favored among other semiconductors [21,22]. The structure and morphology of TiO_2 (nanoparticles [23], nanotubes [24], nanorods [25] and nanofibers [26] can be tuned by modifying the synthesis method, and consequently its electronic and optical properties [27]. Self-organized nanotubes grown using anodization method have a particular interest because they have a high specific surface compared to other nanostructures and they facilitate electron transport between interfaces in a straightforward pathway [28]. The impressive efficiency of highly ordered nanotubes in water splitting, gas sensors, surface-enhanced Raman spectroscopy (SERS) application, biomedical applications, and organic pollutants degradation was demonstrated in various domains [29–33]. However, the nanotubular structure reveals two main drawbacks; the photogenerated electron-hole pairs exhibit a high recombination rate and the material only absorbs UV light, thus reducing its photocatalytic efficiency. To compensate this photocatalytic loss, several solutions have been applied such as coupling TiO_2 with other semiconductors to create heterojunction [15], doping the semiconductor with non-metallic and metallic ions [34] and decorate with plasmonic noble metals [31,35].

The deposition of noble metals (Pd, Au, Pt, Ag) on semiconductors is a method commonly used to improve the photocatalytic activity of the latter. Such contact generates a Schottky barrier which promotes the separation of photogenerated charge carriers in the semiconductor and limits their recombination thus improving photodegradation [36,37]. Additionally, these noble metals are distinguished by

localized surface plasmon resonance (LSPR). This LSPR is a specific visible light absorption resonance, which depends on the nature, size, and shape of the metal nanoparticles [31,38,39]. It was demonstrated elsewhere that the deposition of Pt NPs into TiO_2 enhances its photocatalytic activity in visible light thanks to the created heterojunction that limit charge recombination by the migration of generated electrons to Pt NPs [40,41]. To establish the Pt nanoparticles deposition on the substrate, various synthesis methods have been tested to obtain the optimal metal layer such as photodeposition, electrodeposition, chemical reduction and impregnation reaction [36]. The Pt deposition method holds a significant role because as it was already mentioned the modification on the metal nanoparticle size, shape and dispersion could affect the metal NPs properties [42]. Hence the interest of studying the effect of the deposition method on layer structure in the first instance, and on photocatalytic performance in the second. The photodeposition method used light to deposit NPs onto the substrate which makes it simple and cost-effective method to obtain a uniform deposition. While the electrodeposition method seems more effective towards the formed layer, it allows for better control of thickness and morphology by adjusting the operating parameters such as current density, deposition time and electrolyte composition . In this context, researchers have studied the effect of Pt deposition on photocatalyst efficiency [43,44]. Several studies have shown that varying the amount of deposited platinum directly affects its photocatalytic response [37,45]. Francisco et al. revealed the electrodeposited Pt nanoparticles size that increases from 10 to 250 nm by raising the deposit time [46]. Grabowska and his collaborators have achieved an optimum of photodeposited Pt nanoparticles on TiO_2 for a total Toluene photodegradation [47]. These studies have clearly shown the importance of the deposition method to obtain a uniform metal deposit and avoid nanoparticles agglomeration to the photocatalytic activity.

In this study, we present a new insight regarding the effect of Pt deposition methods onto TiO_2 NTs during the photocatalytic degradation of VOCs (ethyl acetate) and bacteria (Escherichia coli). Pt-NPs are deposed on TiO_2 NTs using two different methods (electrodeposition and photodeposition), then we study the effect of the deposition method on the structural and optical properties of the Pt-NPs. Furthermore, a comparison is highlighted between both deposition methods for the degradation of ethyl acetate (EA) and the simultaneous removal of *E- Coli* and EA.

II. Materials and methods

1. Photocatalyst synthesis: TiO_2-NTs/Pt-NPs

TiO_2 nanotubes anodization

TiO_2 nanotubes (NTs) were grown directly on titanium plates (2.5 cm x 2.5 cm x 1 mm, 99.7%) using anodic oxidation. Prior to anodization, the titanium underwent meticulous polishing and cleaning procedures to facilitate the uniform growth of nanotubes. This involved successive polishing using SiC abrasive papers ranging from grades 320 to 2200. Then, the substrates were cleaned by ultra sonication, first in acetone, then in methanol and finally in distilled water. The elaboration of TiO_2 NTs from Ti substrates involves a two-steps anodization: 45 min for the first anodization and 120 min for the second one under a fixed voltage of 60 V at room temperature. The process was performed in an electrolyte cell containing 100 ml of ethylene glycol + 1 Wt% NH_4F + 2 v% H_2O. To ensure obtaining the anatase crystal phase of TiO_2, the samples were annealed in an oven at 450 °C for 3 h.

Platinum deposition via the electrodeposition method

Pt deposition was carried in a standard three-electrode electrochemical cell. The electrodes were immersed in 40 mL of 0.5 M of H_2SO_4 + 0.5 mM of H_2PtCl_6 solution. Then, using the potentiostatic method, the electrodeposition was carried out at room temperature under a potential of -0.2 V. Under similar operating conditions, the Pt deposition time was varied (60s, 120s, 180s, 240s).

Platinum deposition via Photodeposition method

The Pt NPs were deposited onto the TiO_2 nanotubes using an aqueous solution composed of 2 mM $H_2PtCl_6 \cdot 6H_2O$ and 50% w/v methanol. The mixture is then placed in a quartz cell containing the TiO_2 NTs – based electrode and irradiated at room temperature by a Puritec germicidal lamp (HNS 15 W G13) that emit high intensity UVC irradiation with a dominant wavelength around 254 nm during 30 min, 1h, 2h, 3h, 4h. Finally, the electrode was rinsed with MQ water and dried under N_2 flow.

2. Photocatalyst characterization

To examine the morphology of the prepared samples, we utilized a 15 kV Scanning Electron Microscope (SEM, Q250) equipped with X-ray energy-dispersive analysis (EDX), as well as a 200 kV Transmission Electron Microscope (TEM) Jeol JEM 2100 HR, coupled with a CCD (Gatan Orius SC200D). For characterization of the crystalline structure, X-ray diffraction (XRD) employing CuKα irradiation (λ = 1.5406 Å) was conducted using a Philips X'PERTMPD instrument. Photoluminescence (PL) measurements were performed using a PerkinElmer spectrometer (LS55) paired with a xenon lamp (wavelength = 340 nm).

3. Target pollutants and reactor for VOC and bacteria removal

The photocatalytic efficiency of the prepared photocatalysts was tested for simultaneous removal of Ethyl Acetate (EA) and bacteria (*Escherichia Coli* strain (DSM 10198–0307-001*E. Coli*). EA is mainly used in paints, printing inks, plastics, organic synthesis, and mostly in agri-food industry.

The degradation of both VOC and bacterial are tested in a batch reactor. The experiments are carried out for individual and mixture of pollutants. For all experiments, the active surface area of the photocatalyst is fixed at 2x2 cm^2. The 250 mL reactor was illuminated using a visible lamp (Sylvania Lynx-S 9W/840) which emits white light with a wavelength between 400 and 700 nm.

4. Photocatalytic degradation of Ethyl Acetate and bacterial

The EA removal, in a batch reactor, was carried out at with different concentrations (5, 10, 15 and 20 mg/m^3) under similar operating conditions. The photocatalyst is placed in the 250 mL batch reactor equipped with a stopper surmounted by a septum and closed hermetically. A known volume of the Ethyl Acetate is then introduced into the reactor and equilibrated for 15 min. Then, the visible light lamp was turned on to activate the of photocatalysis reaction. The reaction aliquot was collected each 5 min, and the degradation efficiency was monitored by Gas Chromatography (GC). For bacterial removal study, 100 µL solution was placed on the photocatalyst, then the visible light was applied for defined period. The deactivation kinetics of bacteria is then studied. The preparation of the bacterial strains and the batch reactor were well detailed in a previous work [48,49].

III. Results and discussion

1. XRD analysis

Figure **1** shows XRD patterns of TiO_2-NTs deposited on Pt for both deposition methods. The amorphous structure of the as-grown TiO_2 NTs is transformed into anatase-like TiO_2 NTs subsequent to an annealing at 400°C for 3 hours. The XRD patterns of pure TiO_2 NTs revealed typical anatase diffraction peaks (JCPDS no. 21–1272) with two peaks related to the metallic Titanium substrate (JCPDS no. 44–1294). After Pt deposition on TiO_2 NTs, we observe the appearance of a diffraction peak at $2\boldsymbol{\theta}$ = 40.1° associated to the (111) Pt crystallographic orientation (JCPDS no. 70–2075). Platinum decoration did not affect the crystallographic structure of TiO_2; there is no remarkable change in the position or width of the peaks, which means that there has been no distortion in the TiO_2 anatase structure. The intensity of the Pt-related peak does not increase as deposition time increases for both deposition methods, while it is broader for the photodeposition method. Besides, another platinum peak appears at $2\boldsymbol{\theta}$ = 46.3° related to the (200) Pt crystal orientation, only for the photodeposition method at high deposition times. As already mentioned, the Pt peaks are only observable from a high deposition time for the two deposition methods, but the appearance of the peaks is always clearer and faster for the photodeposition method. So, we can conclude that the photodeposition method is more quantitative.

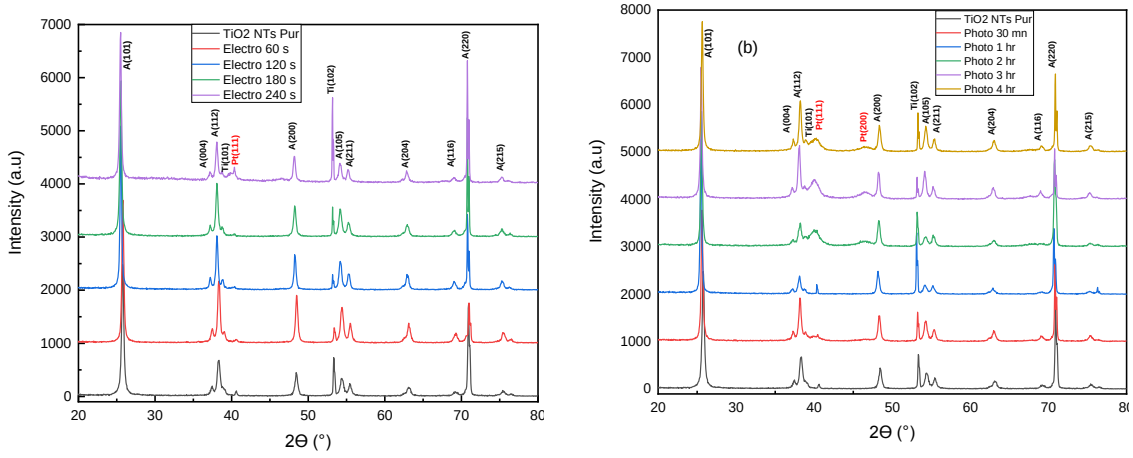

Figure 1: X-ray diffraction patterns of pure TiO_2 NTs and decorated with Pt NPs: (a) Electrodeposition method and (b) Photodeposition method.

2. MEB and EDX analysis

Figure 2 shows SEM images of Pt-decorated TiO_2 NTs corresponding to Pt electrodeposition (**fig. 2a and fig. 2b)** and to Pt photodeposition **(fig. 2c and fig. 2d**), while varying the deposition time. We can see a well-organized nanotubular structure with a tube diameter of around 100 nm. The nanotubular structure has been well studied in a previous work [50]. The EDX analyses are reported in **figures 2 (e-h)**.

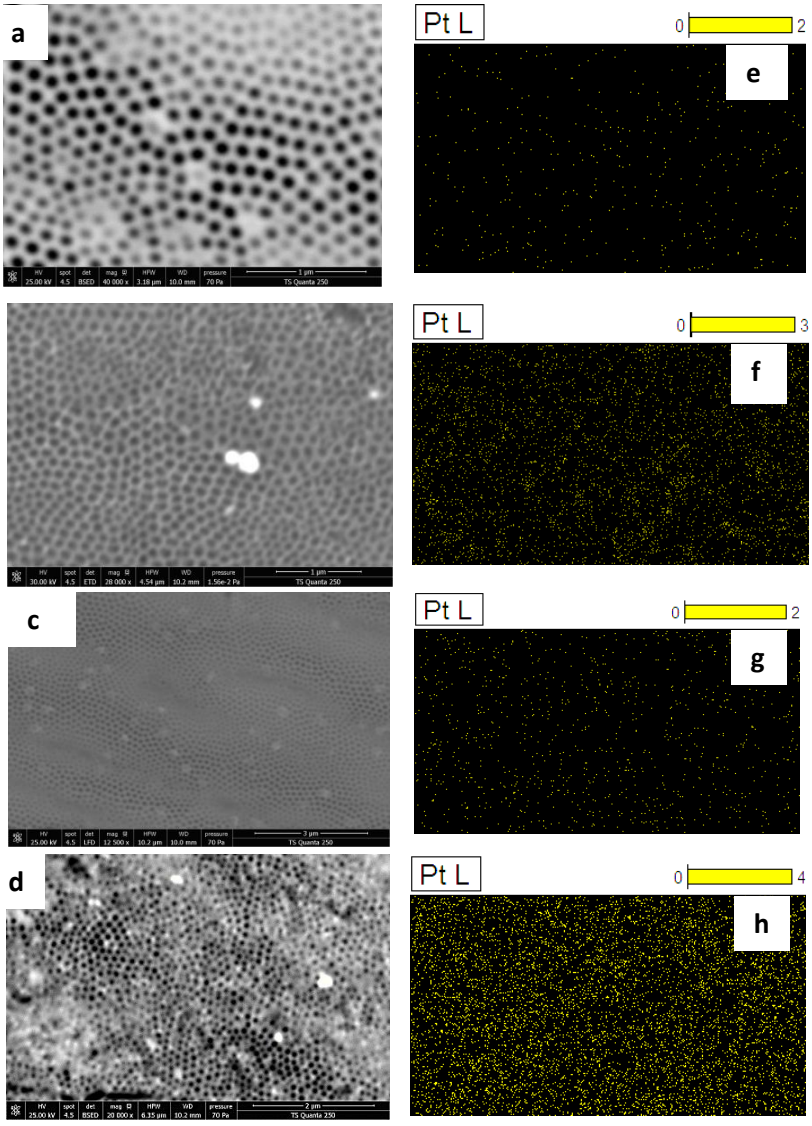

Figure 2: SEM & EDX spectrum of NTs-TiO_2 decorated with NPs-Pt: electrodeposition 120s (a) and 240s (b)), photodeposition 2hr (c) and 4hr (d).

Increasing the electrodeposition time from 120 s (**Figure 2a**) to 240 s (**Figure 2b**) does not result in any significant deformation of the nanotubes. However, EDX mapping shows that the platinum dispersion is uniform on the nanotubular structure.

Since the size of the platinum nanoparticles does not exceed the diameter of the nanotubes (100 nm), the metal nanoparticles are placed on the opening and inside the nanotubes. SEM and EDX mapping clearly show that PT NPs content increases from 0.91 Wt % for Electro-120 s (**fig. 2a**) to 5.58 Wt % for Electro-240 s (**fig. 2b**) (**Table 1**). The increase in photodeposition time from 2 h to 4 hrs more let us obtain more TiO_2 NTs openings covered with agglomerated Pt NPs (**fig. 2d & 2h**). The photodeposition method allows to Pt NPs to condense on the NTs and reached 14.74 Wt % (**Table 1**).

These results confirm the difference between Pt XRD peaks for both decoration methods. The dispersion of Pt NPs is related to the deposition method; electrodeposition is based on the formation of a solid Pt layer on the top of the NTs owing to an electric field so we could control NPs size to prevent the Pt agglomeration. However, photodeposition relies on the use of light to reduce Pt ions could form a massive deposit and in high deposit time the Pt NPs could grow agglomerates that cover the TiO_2 NTs which affect their quantum yield.

Table 1: Platinum weight percentage over deposition time for the two decoration methods.

Photocatalyst	Platinum Wt %		Photocatalyst	Platinum Wt %
Electro 60 s	0.10		Photo 30 min	0.39
Electro 120 s	0.91		Photo 2 hr	5.78
Electro 240 s	5.58		Photo 4 hr	14.74

3. TEM analysis

Transmission electron microscopy show the deposited Pt NPs as black dots (**fig 3a and b**); the electron density of Pt is higher than that of TiO_2. The cross-sectional view of the nanotubes shows that Pt NPs are randomly dispersed under the surface on TiO_2 NTs. The Pt NPs size seems to depend on the deposition method. The size distribution for the two methods prove that Platinum nanoparticles produced via

electrodeposition method are smaller than photodeposition nanoparticles. Indeed, the particles size for Electro 120 s is between 16 and 23 nm, however, Photo 3 h resulted particle size between 27 and 33 nm (**fig 3c and d**).

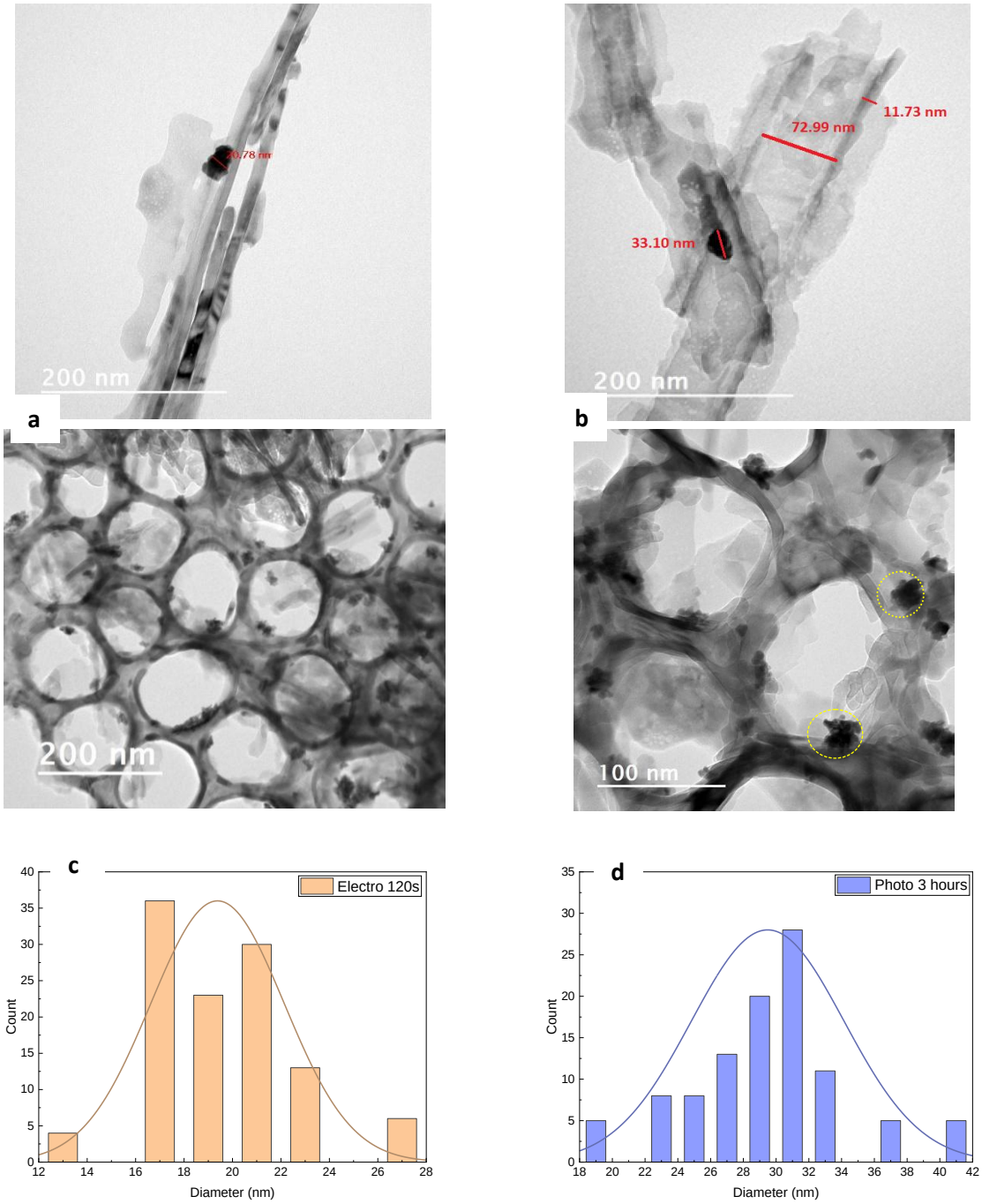

Figure 3: TEM images of the Pt NPs/TiO2 NTs nanocomposite (a) Electro 120 s and (b) Photo 3 hours photocatalysts, size distribution of Platinum nanoparticles (c) Electro 120 s and (d) Photo 3 hours photocatalysts.

4. Photoluminescence analysis

It is necessary to show that the TiO_2-NTs/Pt-NPs junctions pretended to be used, as photocatalysts instead of the pure TiO_2 NTs, are suitable to reduce the electron–hole recombination rate within the photocatalysis process. For this purpose, we measure the PL spectra of the TiO_2-NTs/Pt-NPs photocatalyst. The PL spectra of TiO_2-NTs/Pt-NPs are shown in **figure 4**. The spectra were recorded with an excitation source of 290 nm in ambient conditions.

The PL spectra show several peaks within the 350–600 nm spectral range. While the emission peak at 360 nm corresponds to direct band-to-band transition , the peak at 390 nm corresponds to indirect band-to-band transition [48]. The emission peak at around 435 nm is due to the self-trapped excitons [50]. The emission peaks in the visible range (460 - 540 nm) are due to the electrons trapped in the oxygen vacancy states of the TiO_2 [17]. Generally, the PL is due to the recombination of the photogenerated carriers in a semiconductor. In our case, we observe a visible PL band centered at ~500 nm for TiO_2. This could be ascribed to the recombination of photoexcited electrons and holes possibly due to the oxygen vacancies in TiO_2. When Pt was loaded onto TiO_2 NTs, the intensity of the PL band centered around ~500 nm decreased, suggesting a reduction of the charge carrier recombination rate. This can be explained by the migration of excited electrons from TiO_2 to the Pt NPs and the creation of a Schottky barrier (junction) that limit the electron−hole recombination.

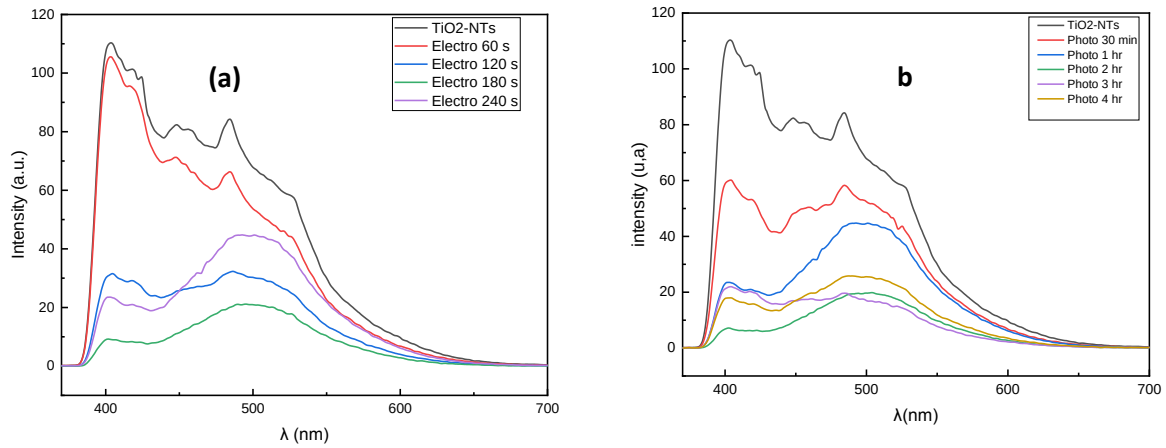

Figure 4: Photoluminescence spectra of TiO_2-NTs decorated with Pt NPs: (a) Electrodeposition method and (b) Photodeposition method.

Photocatalytic application

1. Ethyl Acetate degradation

In order to evaluate the photocatalytic performance of the TiO_2-NTs/Pt-NPs nanocomposites, the degradation of Ethyl Acetate (20 mg/m^3) was studied in a batch reactor under visible light illumination. It is widely recognized that the photodegradation efficiency of noble metal-sensitized TiO_2 varies depending on the deposition method [51]. **Figure 5** illustrates the time-dependent photodegradation of EA, comparing the photocatalytic activity of samples decorated with Pt using both electro and photodeposition methods at various deposition times.

Apparently, in both Pt decoration methods, the addition of Pt NPs improves EA degradation under visible light. In case of pure TiO_2 NTs, the degradation efficiency does not exceed 25% of EA after 240 min of visible light irradiation. Starting with electrodeposition samples **Figure 5a**, the presence of platinum nanoparticles increases sharply EA degradation under visible irradiation. Usually, the photocatalytic efficiency increases with the increase of the deposition time [52].

Which is not the case because the simple with the highest deposition time (Electro 240 s) presents the lowest photocatalytic activity with 65% after 180 minutes of irradiation. However, Electro 120 s sample reaches an elimination percentage of 91% at the same irradiation period with the highest photocatalytic efficiency. With the photodeposition method, the sample (Electro 3 hours) exhibit the best photocatalytic activity comparing other photodeposited samples with an elimination percentage of 70% after 180 minutes of visible irradiation. For all samples, the degradation follows a fall up until 180 minutes of irradiation after that it maintains stability. This phenomenon could be explained by the saturation of active sites caused by the accumulation of intermediate by-products issues from the degradation of EA. Moreover, the accumulation of humidity and excess of oxygen (source of reactive oxygen specie : RSO) can reduce the kinetic of EA degradation [36].

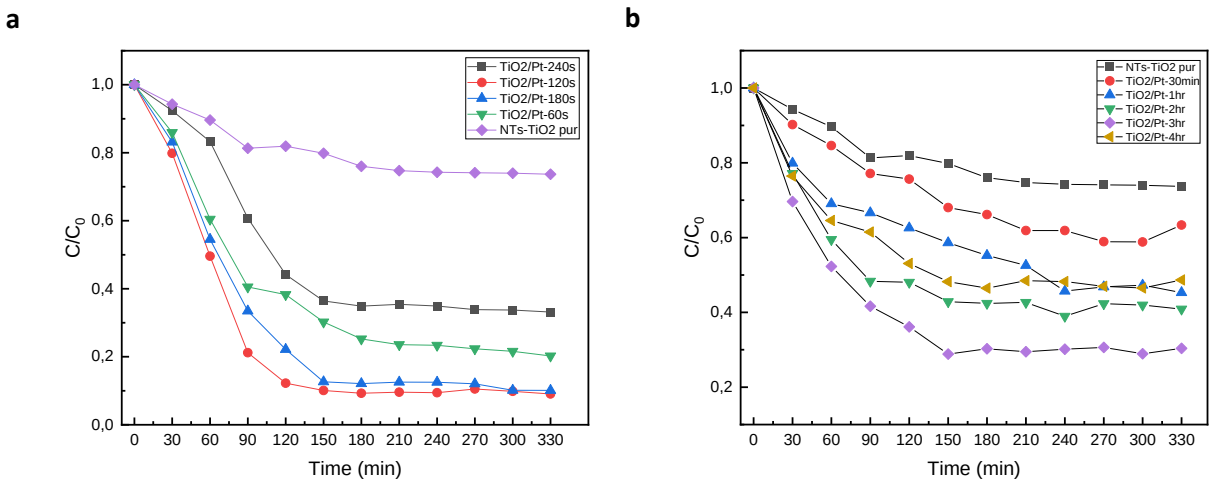

316 **Figure 5: The variation of EA degradation as a function of time of pure and decorated**
317 **TiO_2-NTs by different times of deposition using electrodeposition method (a) and**
318 **Photodeposition method (b).**

319

320 To understand the kinetics of degradation, we variate the initial concentrate of Ethyl
321 Acetate for the most efficient deposition methods (Electro 120 s and Photo 3 h).
322 **Figure 6** shows the variation of EA degradation over irradiation time for different inlet
323 concentrations (5, 10, 15 and 20 mg/m^3). The decrease in the initial concentration
324 implies better degradation of the pollutant and we notice the same behavior for both
325 methods. This is linked to the competition of pollutant molecules on reactive species
326 responsible for the degradation of pollutants [53,54].

327 The behavior of the pollutant during the initial concentration variation is the same for
328 both pollutants. However, the photocatalytic efficiency differs, and the variation of the
329 lowest concentration reaches a total degradation by 120 minutes of visible irradiation
330 for electrodeposition method and after 180 minutes of irradiation for the
331 photodeposition method. Based on the results we could affirm that electrodeposition
332 method exhibits a better photocatalytic activity, but the kinetics depends on several
333 parameters such as the mass of the metal deposited and the nature of dispersion of
334 the platinum. Also, if we relate these results to that of the structural characterizations,
335 we noticed that electrodeposition method presents a better distribution of Platinum
336 nanoparticles with a smaller nanoparticle size which correlates with other works [42].

Lakshamanreddy et al. have proven about 94% degradation of methyl orange dye using chemical reduction method compared to 50.5% using photodeposition method and they related these results to the size of Pt nanoparticles and the oxidation states after Pt deposition [44].

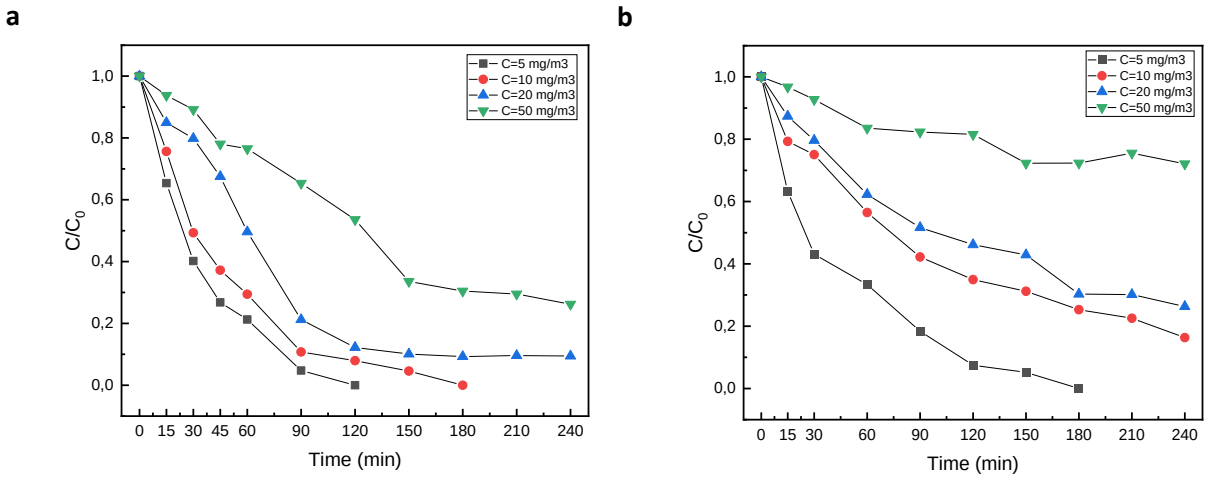

Figure 6: The temporal evolution of EA degradation for different initial concentrations on the photocatalyst Electro 120 s (a) and Photo 3 h (b).

The degradation kinetic of Ethyl acetate can be determined using the Langmuir-Hinshelwood (L-H) model [55,56]:

$$\mathbf{r_0 = -\frac{d[EA]}{dt} = k_c \times \frac{K[EA]_0}{1+K[EA]_0}}$$

where $\mathbf{r_0}$ the initial rate of degradation ($mg.m^{-3}.s^{-1}$).

The values of $\mathbf{r_0}$ are determined using the equations $\mathbf{r_0 = f([EA])}$. The function $\mathbf{1/r_0 = f(1/[EA])}$ is plotted to determine **K**, the adsorption constant and $\mathbf{k_c}$, the kinetic constant. These constants are obtained by linearizing the equation of the L-H model:

$$\frac{1}{r_0} = \frac{1}{K \times k_c} \times \frac{1}{[EA]_0} + \frac{1}{k_c}$$

The L-H model assists the determination of kinetic parameters. We trace the curve $\mathbf{1/r_0 = f(1/[EA])}$ and we have the following results (**Fig 7**):

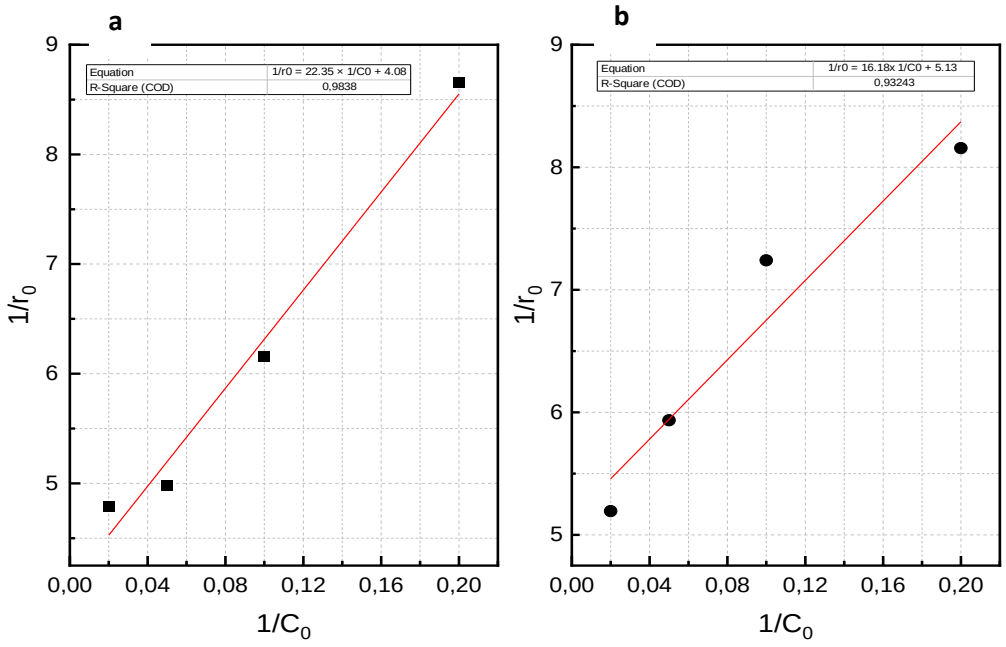

Figure 7: Linear regression using L-H model for EA degradation on Electro 120 s (a) and Photo 3 hours (b) photocatalysts.

Table 2: Adsorption and kinetic constants for the efficient photocatalysts.

	Electro 120 s	**Photo 3 hours**
K: Adsorption Constant of L–H (m^3. mg^{-1})	0.182	0.317
k_c: Kinetic Constant of L–H ($mg.m^{-3}$. s^{-1})	0.245	0.195

The parameters derived from the L-H model are presented in **Table 2**. These results indicate that the Electro 120 s sample exhibits a higher kinetic constant, confirming the superior photocatalytic efficiency of electrodeposited samples. Furthermore, the accuracy of these values is evident as they are consistent with those reported in studies focusing on the degradation of VOCs using photocatalysis.

In **Table 3**, we have compiled additional results pertaining to the treatment of VOCs using photocatalysts based on Pt/TiO_2.

Table 3: Summary of removal efficiency and kinetic constants of VOCs photocatalytic degradation using Titanium dioxide deposit with platinum nanoparticles photocatalysts.

Order	Photocatalyst	Target pollutant	Pollutant concentration (mg/m^3)	Light source	Degradation (%)	Kinetic Constant ($mg.m^{-3}.s^{-1}$)	Reference
1	1%-Pt/TiO_2 prepared by impregnation.	Toluene	5	UV	100	0.86	[57]
2	0.1%-Pt/TiO_2	Ammonia	140	UV	50	0.05	[58]
3	0.3%-Pt/TiO_2 prepared by impregnation.	Benzene	800	UV	100	NA	[59]
4	Pt/TiO_2 prepared by impregnation.	Ethanol	8	UV	100	3.2	[57]
5	0.8%-Pt/TiO_2	Butane	3	NA	27	NA	[60]
6	0.1Pt TiO_2	Toluene	750	UV-Vis	90	NA	[37]
7	Pt/TiO_2 prepared by Electrodeposition.	cyclohexane	8	Visible	100	0.064	[48]
8	0.3%-Pt/TiO_2 prepared by impregnation.	Ethyl Acetate	900	UV	54	NA	[59]
9	Pt/TiO_2 prepared by Photodeposition.	Ethyl Acetate	5	Visible	100	3.25	This work
10	Pt/TiO_2 prepared by Electrodeposition.	Ethyl Acetate	5	Visible	100	5.57	This work

2. Simultaneous removal of EA and bacteria

The efficient photocatalysts were also tested for bacteria (Escherichia coli (E. coli)) inactivation with the presence of Ethyl Acetate. This study could reveal many information such as the ability of elaborated photocatalysts to oxidate more than one pollutant which is the case of indoor air, the effect of presence of many pollutants on the photocatalytic activity and the antibacterial aspect of our photocatalysts. To achieve these objectives, an initial concentration ~2.10^4 (CFU/mL) of E. coli strain was dispersed on the top of photocatalysts. The experiment was carried out on the same batch reactor under visible light.

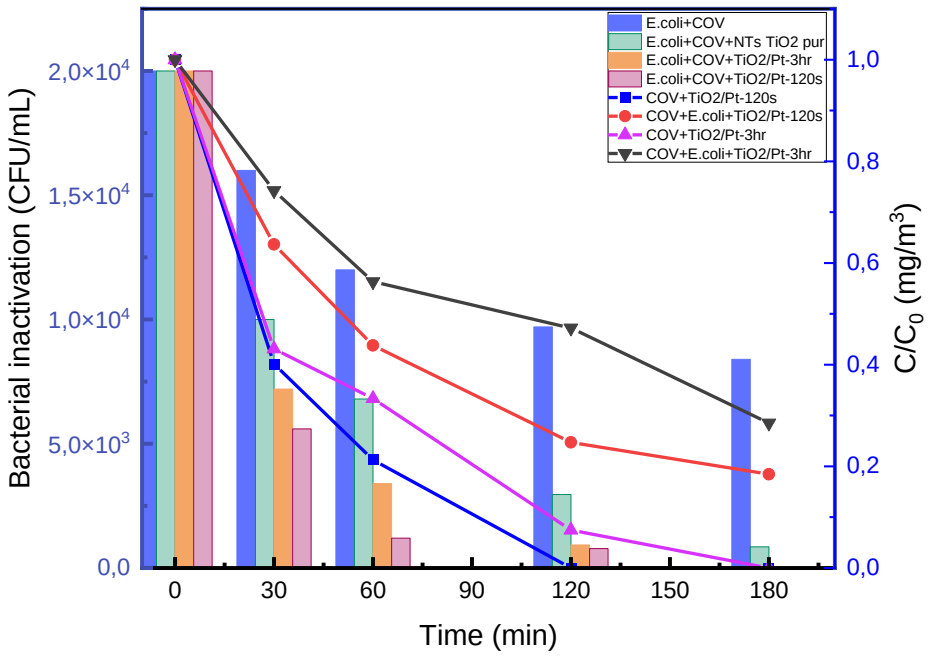

Figure 8: Simultaneous removal of E. Coli and Ethyl Acetate as a function of irradiation time for (i) pure TiO_2 nanotubes, (ii) Electro 120 s and (iii) Photo 3 h photocatalysts.

Figure 8 manifest the simultaneous removal of E. Coli and EA as a function of irradiation time. The bacterial inactivation is presented with the columns, where we can see a downfall of E. Coli concentrations that reaches a total elimination of bacteria for the two efficient photocatalysts by 180 min of visible light irradiation. It should also be mentioned that there is a significant decrease in Bactria and EA with pure TiO_2 nanotubes especially for long duration of visible irradiation. This is studied

by several papers which confirm the antibacterial activity of titanium dioxide under visible light [61,62]. Sunada et al. reports that TiO_2 thin film could damage E. Coli cell membranes and kill the cell by releasing endotoxin [63]. The lines show EA degradation for Electro 120 s and Photo 3 hours with and without the presence of E. Coli. We remark a slight reduce (20%) in the photocatalytic activity with the presence of bacteria. This disturbance is explained by the competition between pollutants over the degradation with reactive oxygen species (ROS) [64]. These generated ROS while the excitation of the semiconductor are responsible for pollutants destruction and its contribution with the active sites of photocatalyst present a major parameter that explain the simultaneous removal behavior.

Thus, the photocatalyst reveal an important antibacterial activity even with the presence of another pollutant. Moreover, the addition of Pt nanoparticles enhanced the performance as reported in other research papers that the addition of noble metals improves the photocatalytic antibacterial activity. **Table 4** summarizes the bacterial removal efficiencies of various reactors.

Table 4: Comparation of E. Coli inactivation using pure and various noble metals decorated TiO_2 photocatalysts.

Photocatalysts	Bacterial initial concentration (CFU/mL)	Type and time of irradiation (min)	Inactivation efficiency (%)	References
TiO_2	10^6	300 minutes of UV light	100%	[64]
Cu_2O/TiO_2	10^8	420 minutes of UV light	100%	[53]
Ag/TiO_2	$2.6\ 10^6$	350 minutes of UV light	100%	[65]
Au/TiO_2	10^5	Visible light	50%	[61]
Pd/TiO_2	10^9	100 minutes of UV light	100%	[66]
Pt/TiO_2	$1.86\ 10^3$	60 minutes of visible light	100%	[48]
	$2\ 10^4$	180 minutes of visible light	100%	This work

3. Plausible Degradation mechanism

The TiO_2 nanotubes exhibited significant photocatalytic activity especially for E. Coli inactivation. However, Pt deposition heavily enhances the photocatalyst performance. As we know, the excitation of TiO_2 could generate many reactive species (OH°, O_2^-) that contribute to the removal of pollutants which explain the photocatalytic efficiency of elaborated nanotubes. Nevertheless, the photocatalytic response of TiO_2 is mostly under UV light which explains the significant improvement by the addition of Pt. The noble metals supplement the photocatalytic response of the semiconductor in visible range [39,67]. Several phenomena can occur when a semiconductor comes into contact with nanoparticles of a noble metal. For instance, the work function of platinum is approximately Φ_M=5.6 eV higher than the electronic affinity of TiO_2 (x_S=3.8 eV). Consequently, when the metal and the semiconductor make contact, the electrons in the semiconductor near the interface possess higher energy levels than those in the metal [40].

A space charge zone therefore appears in the semiconductor with fixed positive ions and the conduction band moves away from the Fermi level in this zone since there are fewer carriers. In this case we have the creation of a Schottky junction (**Figure 9a**) and the generated electrons in the conduction band moves to platinum nanoparticles. Schottky barrier built an electric field in the interface due the charge redistribution which limit the recombination of charge carriers and enhance the photodegradation [44]. The trapped electrons participate in the production of ROS responsible for the degradation of pollutants we therefore understood how the addition of platinum acts on the photocatalytic activity. These generated ROS are strongly oxidative and able to break pollutant molecules. Ethyl acetate breaks in the first place in to CH_3CO, CH_3CH_2 and CH_3COO after that CO_2 and CH_3 molecules were produced by C–C and C–O bonds hemolytic cleavage [68,69]. The plausible EA degradation mechanism is detailed below:

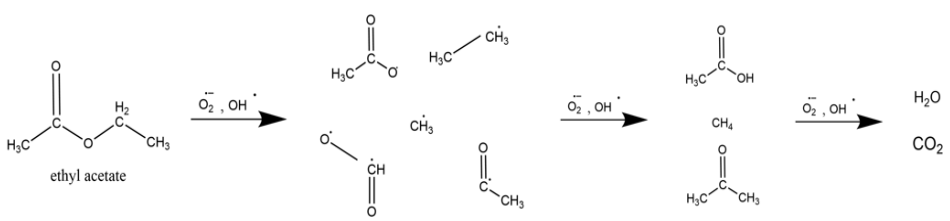

The pathogens inactivation mechanism is mainly based on the DNA destruction and the oxidation of coenzyme A which inhibit the respiratory activities of microorganism. Thus, the photogenerated reactive species leads to cells removal [66,70]. Pigeot-Rémy et al have also reported the membrane destruction of E. coli cells using photocatalytic process. This study highlighted, as shown in TEM image (**Figure 3**), progressive structural changes at the level of the cell wall, due to radical attacks. Along with this observation, it has been shown that when the treatment persists over time, a complete mineralization of the cellular components could take place. Thus, the compounds produced at the end of the reaction would mainly be CO_2, water and minerals [62]. The plausible mechanism of a simultaneous removal of EA and E-coli is summarized in **figure 9**.

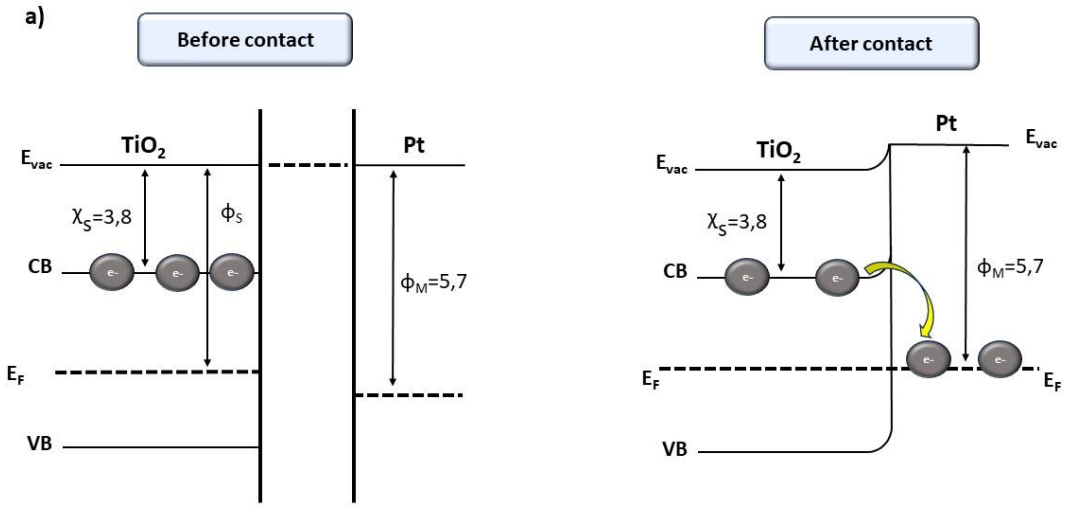

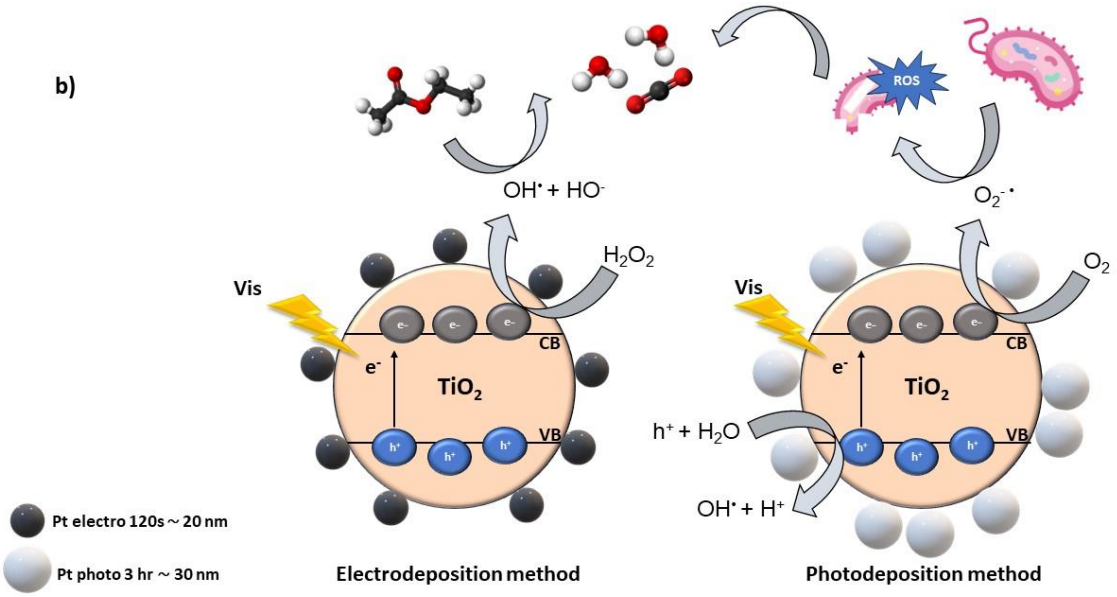

Figure 9: Semiconductor-Metal created junction (a) and degradation mechanism (b).

Conclusions

Summing up, we successfully deposit Platinum nanoparticles onto TiO_2 nanotubes using two different methods. TEM and EDX results confirmed the dispersion of Platinum onto nanotubes with different nanoparticles size ~20 nm for electrodeposition method and ~30 nm for photodeposition method. Then we confirmed the creation of Schottky barrier while the contact between TiO_2 and Pt nanoparticles, which limit the recombination of generated electrons by transferring them from the conduction, band to the metal. Therefore, the effect of platinum deposition was tested on the photocatalytic activity for pollutants degradation. The photodegradation of EA reveal the outperform of the electrodeposition method. Comparing the two efficient photocatalysts Electro 120 s and Photo 3 hours reached a total degradation of Ethyl Acetate under visible irradiation by 120 minutes and 180 minutes respectively. The simultaneous removal of Ethyl Acetate with the presence of bacteria with the efficient photocatalysts showed a slight decrease compared to a single pollutant with a higher bacterial elimination rate for electrodeposition photocatalyst. So, this study has clearly shown that the metal deposit method influences on the structure of the deposited layer and on the size of the nanoparticles which affect their photocatalytic activity.

Acknowledgements

The authors would like to acknowledge the financial support from the Hubert Curien "Utique" partnership of the French Ministry of Europe and Foreign Affairs and the Tunisian Ministry of Higher Education and Scientific Research. AR is also grateful to the University of Tunis El Manar, Tunisia, for providing her with Alternation scholarship for her Research stays at National School of Chemistry of Rennes (ENSCR).

References

[1] C.L. Bianchi, C. Pirola, F. Galli, G. Cerrato, S. Morandi, V. Capucci, Pigmentary TiO2: A challenge for its use as photocatalyst in NOx air purification, Chem. Eng. J. 261 (2015) 76–82. https://doi.org/10.1016/j.cej.2014.03.078.

[2] W. Abou Saoud, A. Kane, P. Le Cann, A. Gerard, L. Lamaa, L. Peruchon, C. Brochier, A. Bouzaza, D. Wolbert, A.A. Assadi, Innovative photocatalytic reactor for the degradation of VOCs and microorganism under simulated indoor air conditions: Cu-Ag/TiO2-based optical fibers at a pilot scale, Chem. Eng. J. 411 (2021) 128622. https://doi.org/10.1016/j.cej.2021.128622.

[3] A.A. ASSADI, A. BOUZAZA, D. WOLBERT, Photocatalyse dans le traitement de l'air, Environnement. (2022). https://doi.org/10.51257/a-v1-g1745.

[4] W. Abou Saoud, A.A. Assadi, M. Guiza, A. Bouzaza, W. Aboussaoud, I. Soutrel, A. Ouederni, D. Wolbert, S. Rtimi, Abatement of ammonia and butyraldehyde under non-thermal plasma and photocatalysis: Oxidation processes for the removal of mixture pollutants at pilot scale, Chem. Eng. J. 344 (2018) 165–172. https://doi.org/10.1016/j.cej.2018.03.068.

[5] Y. Serhane, A. Bouzaza, D. Wolbert, A.A. Assadi, New UV-LED frontal flow photocatalytic reactor for VOCs treatment: Compactness, intensification and optimization studies, Chem. Eng. J. 451 (2023) 138784. https://doi.org/10.1016/j.cej.2022.138784.

[6] A.A. Assadi, A. Bouzaza, S. Merabet, D. Wolbert, Modeling and simulation of VOCs

removal by nonthermal plasma discharge with photocatalysis in a continuous reactor: Synergetic effect and mass transfer, Chem. Eng. J. 258 (2014) 119–127. https://doi.org/10.1016/j.cej.2014.07.050.

[7] N.A. KONE, N. Belkessa, Y. Serhane, S.L. Coulibaly, M. Kamagate, L. Mouni, S. Loganathan, L. Coulibaly, A. Bouzaza, A. Amrane, A.A. Assadi, Chlorobenzene Mineralization Using Plasma/Photocatalysis Hybrid Reactor: Exploiting the Synergistic Effect, Catalysts. 13 (2023) 431. https://doi.org/10.3390/catal13020431.

[8] N. Belkessa, Y. Serhane, A. Bouzaza, L. Khezami, A.A. Assadi, Gaseous ethylbenzene removal by photocatalytic TiO2 nanoparticles immobilized on glass fiber tissue under real conditions: evaluation of reactive oxygen species contribution to the photocatalytic process, Environ. Sci. Pollut. Res. 30 (2022) 35745–35756. https://doi.org/10.1007/s11356-022-24636-8.

[9] Y. Serhane, A. Bouzaza, D. Wolbert, A. Meslem, A.A. Assadi, Smart design for CBRN protection by coupling adsorption and photocatalysis: Regeneration adsorbent efficiency – CWAs' continuous purification, Chem. Eng. J. 471 (2023) 144326. https://doi.org/10.1016/j.cej.2023.144326.

[10] W. Wang, Z. Zhu, C. Wang, F. Zhou, H. Yu, Y. Zhang, W. Zhou, J. Yang, Q. Zhu, Y. Chen, S. Pan, W. Yan, L. Wang, Post-drying decontamination of laver by dielectric barrier discharge plasma, UV radiation, ozonation, and hot air treatments, LWT. 176 (2023) 114518. https://doi.org/10.1016/j.lwt.2023.114518.

[11] N. Belkessa, A. Bouzaza, A.A. Assadi, Understanding of the synergy effect of DBD plasma discharge combined to photocatalysis in the case of Ethylbenzene removal: Interaction between plasma reactive species and catalyst, J. Environ. Chem. Eng. 11 (2023) 110640. https://doi.org/10.1016/j.jece.2023.110640.

[12] L. Zhang, M. Jaroniec, Toward designing semiconductor-semiconductor heterojunctions for photocatalytic applications, Appl. Surf. Sci. 430 (2018) 2–17. https://doi.org/10.1016/j.apsusc.2017.07.192.

[13] A. FUJISHIMA, K. HONDA, Electrochemical Photolysis of Water at a Semiconductor Electrode, Nature. 238 (1972) 37–38. https://doi.org/10.1038/238037a0.

[14] J. Hammouche, K. Daoudi, S. Columbus, R. Ziad, K. Ramachandran, M. Gaidi, Structural and morphological optimization of Ni doped ZnO decorated silicon nanowires for photocatalytic degradation of methylene blue, Inorg. Chem. Commun. 131 (2021) 108763. https://doi.org/10.1016/j.inoche.2021.108763.

[15] A. Hajjaji, S. Jemai, A. Rebhi, K. Trabelsi, M. Gaidi, A.N. Alhazaa, M.A. Al-Gawati, M.A. El Khakani, B. Bessais, Enhancement of photocatalytic and photoelectrochemical properties of TiO2 nanotubes sensitized by SILAR - Deposited PbS nanoparticles, J. Mater. 6 (2020) 62–69. https://doi.org/10.1016/j.jmat.2019.12.002.

[16] M. Gaidi, A. Hajjaji, R. Smirani, B. Bessais, M.A. El Khakani, Structure and photoluminescence of ultrathin films of SnO2 nanoparticles synthesized by means of pulsed laser deposition, J. Appl. Phys. 108 (2010). https://doi.org/10.1063/1.3485811.

[17] S. Sassi, K. Trabelsi, A. El Jery, M. Abidi, A. Hajjaji, L. Khezami, A. Karrech, M. Gaidi, B.M. Soucase, B. Bessais, Synergistic effect of CuxOy-NPs/TiO2-NTs heterostructure on the photodegradation of amido black staining, Optik (Stuttg). 272 (2023) 170234. https://doi.org/10.1016/j.ijleo.2022.170234.

[18] S. Jemai, L. Khezami, K. Gueddana, K. Trabelsi, A. Hajjaji, M. Amlouk, B.M. Soucase, B. Bessais, S. Rtimi, Impact of Annealing on ZrO2 Nanotubes for Photocatalytic Application, Catalysts. 13 (2023) 558. https://doi.org/10.3390/catal13030558.

[19] Y. Boyjoo, H. Sun, J. Liu, V.K. Pareek, S. Wang, A review on photocatalysis for air treatment: From catalyst development to reactor design, Chem. Eng. J. 310 (2017) 537–559. https://doi.org/10.1016/j.cej.2016.06.090.

[20] A.A. Assadi, O. Baaloudj, L. Khezami, N. Ben Hamadi, L. Mouni, A.A. Assadi, A. Ghorbal, An Overview of Recent Developments in Improving the Photocatalytic Activity of TiO2-Based Materials for the Treatment of Indoor Air and Bacterial Inactivation, Materials (Basel). 16 (2023) 2246. https://doi.org/10.3390/ma16062246.

[21] Y. Zhao, N. Hoivik, K. Wang, Recent advance on engineering titanium dioxide nanotubes for photochemical and photoelectrochemical water splitting, Nano Energy. 30 (2016) 728–744. https://doi.org/10.1016/j.nanoen.2016.09.027.

[22] H. Dhiflaoui, M.A. Hajjaji, A. Hajjaji, L. Khezami, A. Karrech, B. Bessais, A. Ben Cheikh Larbi, M. Amlouk, Enhanced Interfacial Adhesion of TiO2 Nanotubes Decorated With Ag Silver Nanoparticles Prepared by Photo-Reduction Process, J. Tribol. 145 (2023). https://doi.org/10.1115/1.4062485.

[23] M. Ismael, A review and recent advances in solar-to-hydrogen energy conversion based on photocatalytic water splitting over doped-TiO2 nanoparticles, Sol. Energy. 211 (2020) 522–546. https://doi.org/10.1016/j.solener.2020.09.073.

[24] M. Krbal, S. Ng, M. Motola, L. Hromadko, F. Dvorak, V. Prokop, H. Sopha, J.M. Macak, Sulfur treated 1D anodic TiO2 nanotube layers for significant photo- and

electroactivity enhancement, Appl. Mater. Today. 17 (2019) 104–111. https://doi.org/10.1016/j.apmt.2019.07.018.

[25] T. Gupta, Samriti, J. Cho, J. Prakash, Hydrothermal synthesis of TiO2 nanorods: formation chemistry, growth mechanism, and tailoring of surface properties for photocatalytic activities, Mater. Today Chem. 20 (2021) 100428. https://doi.org/10.1016/j.mtchem.2021.100428.

[26] J. Song, R. Guan, M. Xie, P. Dong, X. Yang, J. Zhang, Advances in electrospun TiO2 nanofibers: Design, construction, and applications, Chem. Eng. J. 431 (2022) 134343. https://doi.org/10.1016/j.cej.2021.134343.

[27] K. Trabelsi, A. Hajjaji, I. Ka, M. Gaidi, B. Bessais, M.A. El Khakani, Optoelectronic and photocatalytic properties of in situ platinum-doped TiO2 films deposited by means of pulsed laser ablation technique, J. Mater. Sci. Mater. Electron. 28 (2017) 3317–3324. https://doi.org/10.1007/s10854-016-5925-z.

[28] D. Chen, Y. Cheng, N. Zhou, P. Chen, Y. Wang, K. Li, S. Huo, P. Cheng, P. Peng, R. Zhang, L. Wang, H. Liu, Y. Liu, R. Ruan, Photocatalytic degradation of organic pollutants using TiO2-based photocatalysts: A review, J. Clean. Prod. 268 (2020) 121725. https://doi.org/10.1016/j.jclepro.2020.121725.

[29] M. Gaidi, K. Trabelsi, A. Hajjaji, M.L. Chourou, A.N. Alhazaa, B. Bessais, M.A. El Khakani, Optimizing the photochemical conversion of UV–vis light of silver-nanoparticles decorated TiO 2 nanotubes based photoanodes, Nanotechnology. 29 (2018) 015703. https://doi.org/10.1088/1361-6528/aa96c3.

[30] H. Abe, Y. Kimura, T. Ma, D. Tadaki, A. Hirano-Iwata, M. Niwano, Response characteristics of a highly sensitive gas sensor using a titanium oxide nanotube film decorated with platinum nanoparticles, Sensors Actuators B Chem. 321 (2020) 128525. https://doi.org/10.1016/j.snb.2020.128525.

[31] J. Jimenez-Cisneros, J.P. Galindo-Lazo, M.A. Mendez-Rojas, J.R. Campos-Delgado, M. Cerro-Lopez, Plasmonic Spherical Nanoparticles Coupled with Titania Nanotube Arrays Prepared by Anodization as Substrates for Surface-Enhanced Raman Spectroscopy Applications: A Review, Molecules. 26 (2021) 7443. https://doi.org/10.3390/molecules26247443.

[32] A. Hajjaji, K. Trabelsi, A. Atyaoui, M. Gaidi, L. Bousselmi, B. Bessais, M.A. El Khakani, Photocatalytic activity of Cr-doped TiO2 nanoparticles deposited on porous multicrystalline silicon films, Nanoscale Res. Lett. 9 (2014) 543.

https://doi.org/10.1186/1556-276X-9-543.

[33] L. Mohan, C. Dennis, N. Padmapriya, C. Anandan, N. Rajendran, Effect of Electrolyte Temperature and Anodization Time on Formation of TiO2 Nanotubes for Biomedical Applications, Mater. Today Commun. 23 (2020) 101103. https://doi.org/10.1016/j.mtcomm.2020.101103.

[34] Y.-K. Lai, J.-Y. Huang, H.-F. Zhang, V.-P. Subramaniam, Y.-X. Tang, D.-G. Gong, L. Sundar, L. Sun, Z. Chen, C.-J. Lin, Nitrogen-doped TiO2 nanotube array films with enhanced photocatalytic activity under various light sources, J. Hazard. Mater. 184 (2010) 855–863. https://doi.org/10.1016/j.jhazmat.2010.08.121.

[35] A. Pearson, H. Zheng, K. Kalantar-zadeh, S.K. Bhargava, V. Bansal, Decoration of TiO 2 Nanotubes with Metal Nanoparticles Using Polyoxometalate as a UV-Switchable Reducing Agent for Enhanced Visible and Solar Light Photocatalysis, Langmuir. 28 (2012) 14470–14475. https://doi.org/10.1021/la3033989.

[36] A. Esrafili, M. Salimi, A. jonidi jafari, H. Reza Sobhi, M. Gholami, R. Rezaei Kalantary, Pt-based TiO2 photocatalytic systems: A systematic review, J. Mol. Liq. 352 (2022) 118685. https://doi.org/10.1016/j.molliq.2022.118685.

[37] E. Grabowska, M. Marchelek, T. Klimczuk, G. Trykowski, A. Zaleska-Medynska, Noble metal modified TiO2 microspheres: Surface properties and photocatalytic activity under UV–vis and visible light, J. Mol. Catal. A Chem. 423 (2016) 191–206. https://doi.org/10.1016/j.molcata.2016.06.021.

[38] W. Hou, S.B. Cronin, A Review of Surface Plasmon Resonance-Enhanced Photocatalysis, Adv. Funct. Mater. 23 (2013) 1612–1619. https://doi.org/10.1002/adfm.201202148.

[39] C. Vanlalhmingmawia, S.M. Lee, D. Tiwari, Plasmonic noble metal doped titanium dioxide nanocomposites: Newer and exciting materials in the remediation of water contaminated with micropollutants, J. Water Process Eng. 51 (2023) 103360. https://doi.org/10.1016/j.jwpe.2022.103360.

[40] M. Zare, A. Mortezaali, A. Shafiekhani, Photoelectrochemical Determination of Shallow and Deep Trap States of Platinum-Decorated TiO 2 Nanotube Arrays for Photocatalytic Applications, J. Phys. Chem. C. 120 (2016) 9017–9027. https://doi.org/10.1021/acs.jpcc.5b11987.

[41] G. Xu, H. Liu, J. Wang, J. Lv, Z. Zheng, Y. Wu, Photoelectrochemical Performances and Potential Applications of TiO2 Nanotube Arrays Modified with Ag and Pt

610 Nanoparticles, Electrochim. Acta. 121 (2014) 194–202.
611 https://doi.org/10.1016/j.electacta.2013.12.154.

612 [42] D. Wang, Z.-P. Liu, W.-M. Yang, Revealing the Size Effect of Platinum Cocatalyst for
613 Photocatalytic Hydrogen Evolution on TiO 2 Support: A DFT Study, ACS Catal. 8
614 (2018) 7270–7278. https://doi.org/10.1021/acscatal.8b01886.

615 [43] E. Gharibshahi, E. Saion, Influence of dose on particle size and optical properties of
616 colloidal platinum nanoparticles, Int. J. Mol. Sci. 13 (2012) 14723–14741.
617 https://doi.org/10.3390/ijms131114723.

618 [44] N. Lakshmanareddy, V. Navakoteswara Rao, K.K. Cheralathan, E.P. Subramaniam,
619 M.V. Shankar, Pt/TiO2 nanotube photocatalyst – Effect of synthesis methods on
620 valance state of Pt and its influence on hydrogen production and dye degradation, J.
621 Colloid Interface Sci. 538 (2019) 83–98. https://doi.org/10.1016/j.jcis.2018.11.077.

622 [45] L.C. Almeida, M.V.B. Zanoni, Decoration of Ti/TiO 2 Nanotubes with Pt Nanoparticles
623 for Enhanced UV-Vis Light Absorption in Photoelectrocatalytic Process, J. Braz.
624 Chem. Soc. 25 (2014) 579–588. https://doi.org/10.5935/0103-5053.20140034.

625 [46] F.A. Filippin, M.I. Rojas, L.B. Avalle, Electrochemical and microscopic characterization
626 of titanium dioxide electrodes modified with platinum nanoparticles, J. Electroanal.
627 Chem. 946 (2023) 117717. https://doi.org/10.1016/j.jelechem.2023.117717.

628 [47] E. Grabowska, M. Marchelek, T. Klimczuk, G. Trykowski, A. Zaleska-Medynska, Noble
629 metal modified TiO2 microspheres: Surface properties and photocatalytic activity
630 under UV–vis and visible light, J. Mol. Catal. A Chem. 423 (2016) 191–206.
631 https://doi.org/10.1016/j.molcata.2016.06.021.

632 [48] L. Khezami, I. Lounissi, A. Hajjaji, A. Guesmi, A.A. Assadi, B. Bessais, Synthesis and
633 characterization of tio2 nanotubes (Tio2-nts) decorated with platine nanoparticles (pt-
634 nps): Photocatalytic performance for simultaneous removal of microorganisms and
635 volatile organic compounds, Materials (Basel). 14 (2021).
636 https://doi.org/10.3390/ma14237341.

637 [49] M. Abidi, A.A. Assadi, A. Bouzaza, A. Hajjaji, B. Bessais, S. Rtimi, Photocatalytic
638 indoor/outdoor air treatment and bacterial inactivation on CuxO/TiO2 prepared by
639 HiPIMS on polyester cloth under low intensity visible light, Appl. Catal. B Environ. 259
640 (2019) 118074. https://doi.org/10.1016/j.apcatb.2019.118074.

641 [50] M.A. Hajjaji, K. Missaoui, K. Trabelsi, A. Bouzaza, B. Bessais, A. Hajjaji, A.A. Assadi,
642 Electrodeposited Platinum Nanoparticles on Highly Ordered Titanium Dioxide

643 Nanotubes for Photocatalytic Application: Enhancement of Photocatalytic Degradation
644 of Amido Black Dye, Catal. Letters. (2023). https://doi.org/10.1007/s10562-023-04380-
645 5.

646 [51] A. Gołąbiewska, W. Lisowski, M. Jarek, G. Nowaczyk, M. Michalska, S. Jurga, A.
647 Zaleska-Medynska, The effect of metals content on the photocatalytic activity of TiO2
648 modified by Pt/Au bimetallic nanoparticles prepared by sol-gel method, Mol. Catal. 442
649 (2017) 154–163. https://doi.org/10.1016/j.mcat.2017.09.004.

650 [52] X. Yang, Z. Chen, D. Zhou, W. Zhao, X. Qian, Q. Yang, T. Sun, C. Shen, Ultra-low
651 Au–Pt Co-decorated TiO2 nanotube arrays: Construction and its improved visible-
652 light-induced photocatalytic properties, Sol. Energy Mater. Sol. Cells. 201 (2019)
653 110065. https://doi.org/10.1016/j.solmat.2019.110065.

654 [53] M. Abidi, A. Hajjaji, A. Bouzaza, K. Trablesi, H. Makhlouf, S. Rtimi, A.A. Assadi, B.
655 Bessais, Simultaneous removal of bacteria and volatile organic compounds on Cu2O-
656 NPs decorated TiO2 nanotubes: Competition effect and kinetic studies, J. Photochem.
657 Photobiol. A Chem. 400 (2020) 112722.
658 https://doi.org/10.1016/j.jphotochem.2020.112722.

659 [54] A.A. Assadi, J. Palau, A. Bouzaza, J. Penya-Roja, V. Martinez-Soriac, D. Wolbert,
660 Abatement of 3-methylbutanal and trimethylamine with combined plasma and
661 photocatalysis in a continuous planar reactor, J. Photochem. Photobiol. A Chem. 282
662 (2014) 1–8. https://doi.org/10.1016/j.jphotochem.2014.03.001.

663 [55] L. Mouni, L. Belkhiri, J.-C. Bollinger, A. Bouzaza, A. Assadi, A. Tirri, F. Dahmoune, K.
664 Madani, H. Remini, Removal of Methylene Blue from aqueous solutions by adsorption
665 on Kaolin: Kinetic and equilibrium studies, Appl. Clay Sci. 153 (2018) 38–45.
666 https://doi.org/10.1016/j.clay.2017.11.034.

667 [56] A.A. Assadi, A. Bouzaza, D. Wolbert, Study of synergetic effect by surface discharge
668 plasma/TiO2 combination for indoor air treatment: Sequential and continuous
669 configurations at pilot scale, J. Photochem. Photobiol. A Chem. 310 (2015) 148–154.
670 https://doi.org/10.1016/j.jphotochem.2015.05.007.

671 [57] V.P. Santos, S.A.C. Carabineiro, P.B. Tavares, M.F.R. Pereira, J.J.M. Órfão, J.L.
672 Figueiredo, Oxidation of CO, ethanol and toluene over TiO2 supported noble metal
673 catalysts, Appl. Catal. B Environ. 99 (2010) 198–205.
674 https://doi.org/10.1016/j.apcatb.2010.06.020.

675 [58] G.J. Kim, D.W. Kwon, J.H. Shin, K.W. Kim, S.C. Hong, Influence of the addition of

676 vanadium to Pt/TiO 2 catalyst on the selective catalytic oxidation of NH 3 to N 2,
677 Environ. Technol. 40 (2019) 2588–2600.
678 https://doi.org/10.1080/09593330.2018.1554004.

679 [59] P. Papaefthimiou, T. Ioannides, X.E. Verykios, Performance of doped Pt/TiO2 (W6+)
680 catalysts for combustion of volatile organic compounds (VOCs), Appl. Catal. B
681 Environ. 15 (1998) 75–92. https://doi.org/10.1016/S0926-3373(97)00038-6.

682 [60] Y.-F.Y. Yao, Oxidation of Alkanes over Noble Metal Catalysts, Ind. Eng. Chem. Prod.
683 Res. Dev. 19 (1980) 293–298. https://doi.org/10.1021/i360075a003.

684 [61] K.-S. Moon, E.-J. Choi, J.-M. Bae, Y.-B. Park, S. Oh, Visible Light-Enhanced
685 Antibacterial and Osteogenic Functionality of Au and Pt Nanoparticles Deposited on
686 TiO2 Nanotubes, Materials (Basel). 13 (2020) 3721.
687 https://doi.org/10.3390/ma13173721.

688 [62] S. Pigeot-Rémy, F. Simonet, E. Errazuriz-Cerda, J.C. Lazzaroni, D. Atlan, C. Guillard,
689 Photocatalysis and disinfection of water: Identification of potential bacterial targets,
690 Appl. Catal. B Environ. 104 (2011) 390–398.
691 https://doi.org/10.1016/j.apcatb.2011.03.001.

692 [63] K. Sunada, Y. Kikuchi, K. Hashimoto, A. Fujishima, Bactericidal and Detoxification
693 Effects of TiO 2 Thin Film Photocatalysts, Environ. Sci. Technol. 32 (1998) 726–728.
694 https://doi.org/10.1021/es970860o.

695 [64] K. Trabelsi, M. Abidi, A. Hajjaji, R. Tefdini, B. Bessais, S. Rtimi, Photoelectrochemical
696 properties and reactivity of supported titanium NTs for bacterial inactivation and
697 organic pollutant removal, Environ. Sci. Pollut. Res. 30 (2022) 10733–10744.
698 https://doi.org/10.1007/s11356-022-22923-y.

699 [65] M. Abidi, W. Abou Saoud, A. Bouzaza, A. Hajjaji, B. Bessais, D. Wolbert, A.A. Assadi,
700 S. Rtimi, Dynamics of VOCs degradation and bacterial inactivation at the interface of
701 AgxO/Ag/TiO2 prepared by HiPIMS under indoor light, J. Photochem. Photobiol. A
702 Chem. 435 (2023) 114321. https://doi.org/10.1016/j.jphotochem.2022.114321.

703 [66] P. Wu, J.A. Imlay, J.K. Shang, Mechanism of Escherichia coli inactivation on
704 palladium-modified nitrogen-doped titanium dioxide, Biomaterials. 31 (2010) 7526–
705 7533. https://doi.org/10.1016/j.biomaterials.2010.06.032.

706 [67] J. Jimenez-Cisneros, J.P. Galindo-Lazo, M.A. Mendez-Rojas, J.R. Campos-Delgado,
707 M. Cerro-Lopez, Plasmonic Spherical Nanoparticles Coupled with Titania Nanotube
708 Arrays Prepared by Anodization as Substrates for Surface-Enhanced Raman

709 Spectroscopy Applications: A Review, Molecules. 26 (2021) 7443.
710 https://doi.org/10.3390/molecules26247443.

711 [68] J. Li, S. Mo, X. Ding, L. Huang, X. Zhou, Y. Fan, Y. Zhang, M. Fu, Q. Xie, D. Ye,
712 Hollow cavity engineering of MOFs-derived hierarchical MnOx structure for highly
713 efficient photothermal degradation of ethyl acetate under light irradiation, Chem. Eng.
714 J. 464 (2023) 142412. https://doi.org/10.1016/j.cej.2023.142412.

715 [69] H. Wang, S. Chen, Z. Wang, Y. Zhou, Z. Wu, A novel hybrid Bi2MoO6-MnO2 catalysts
716 with the superior plasma induced pseudo photocatalytic-catalytic performance for ethyl
717 acetate degradation, Appl. Catal. B Environ. 254 (2019) 339–350.
718 https://doi.org/10.1016/j.apcatb.2019.05.018.

719 [70] T.O. Ajiboye, S.O. Babalola, D.C. Onwudiwe, Photocatalytic Inactivation as a Method
720 of Elimination of E. coli from Drinking Water, Appl. Sci. 11 (2021) 1313.
721 https://doi.org/10.3390/app11031313.

722